Flat tie-line power scheduling control of grid-connected hybrid microgrids

Xiao, Zhao xia; Guerrero, Josep M.; Shuang, Jia; Sera, Dezso; Schaltz, Erik; Vásquez, Juan C.

Published in:
Applied Energy

DOI (link to publication from Publisher):
10.1016/j.apenergy.2017.07.066

Publication date:
2018

Document Version
Early version, also known as pre-print

Flat Tie-line Power Scheduling Control of Grid-Connected Hybrid Microgrids

Xiao Zhao-xia[*1], Josep M. Guerrero[2], Jia Shuang[3] ,Dezso Sera[2], Erik Schaltz[2], Juan C. Vásquez[2]

1. Tianjin Key Laboratory of Advanced Electrical Engineering and Energy Technology, Tianjin Polytechnic University, Tianjin, 300387, P. R. China
2. Dept. Energy Technology, Aalborg University, Denmark, joz@et.aau.dk , www.microgrids.et.aau.dk
3. Goldwind Science & Technology Co., Ltd. 8 BoXing 1st Road, Economic & Technological Development Zone, Yizhuang, Beijing, 100176,P. R. China

* Corresponding author
xiaozhaoxia@tjpu.edu.cn

Keywords

Grid-connected hybrid microgrids, tie-line power flow, flat power scheduling, hierarchical coordination control, central controller, local controller

Acronyms

Wind turbine (WT), photovoltaic (PV), energy storage units (ESUs), microgrids (MGs), distributed generation (DG), maximum power point tracking (MPPT), active distribution networks (ADN), active power (*P*), reactive power (*Q*), doubly-fed induction generator (DFIG), energy management system (EMS)

Nomenclature

Parameter	***Description***
C	Usable capacity of the battery [Ah]
$D_{\text{dutycycle}}$	Duty cycle of the DC/DC converter [%]
I_{bat}	Battery current [A]
I_{Cmin}	Maximum charge current of the battery [A]
I_{Dmax}	Maximum discharge current of the battery [A]
K_{β}	A proportional coefficient of pitch control [-]
P_B	Active power of ESU [W]
P_{gl}	Output power of MG [W]
P_{inv}	Output active power of PV-inverter [W]
P_{mpp}	Maximum output power of PV at certain irradiation [W]
P_{PV}	Active power of PV [W]
P_r	Active power of DFIG rotor-side [W]
P_{REF}	Active power reference of PV-inverter [W]
P_s	Active power of DFIG stator-side [W]

P_T	Average power during the dispatching time T [W]
P_T^*	Output power reference of MG during T [W]
P_W	Active power of WT [W]
P_w^*	Power reference of WT [W]
P_{wmax}*	Maximum power at a certain wind speed [W]
Q_{REF}	Reactive power reference of PV-inverter [var]
SoC	State of charge of the battery
$SoC(0)$	Initial SoC of the battery [%]
T	Dispatching time [s]
v	Wind speed [m/s]
V_{bat}	Battery voltage [V]
V_{DClink}	DC bus voltage of the PV array [V]
v_{max}	Maximum (cut-out) wind speed [m/s]
v_{min}	Minimum (cut-in) wind speed [m/s]
V_{mpp}	Maximum power point voltage of the PV array at certain irradiation [V]
V_{OC}	Open circuit voltage of the PV array [V]
V_{th}	Threshold battery voltage [V]
W_{PV}	Electric energy generated by the PV array [W·s]
τ_β	Time constant of the pitch actuator [s]
β	Pitch angle of the WT [°]
β^*	Pitch angle reference of the WT [°]

Abstract

In future active distribution networks (ADNs), microgrids (MGs) may have the possibility to control the power dispatched to the ADN by coordinating the output power of their multiple renewable generation units and energy storage units (ESUs). In this way, each MG may support the active distribution network, while promoting the penetration of renewable energy sources in a rational way. In this paper, we propose a tie-line power flow control of a hybrid MG, including photovoltaic (PV) generator, small wind turbines (WT), and ESUs.

Firstly, the structure of the hybrid PV/WT/ESU MG is presented. In this power architecture, the battery is directly connected to the PV side through a DC/DC converter, thus reducing the number of conversions. Secondly, a hierarchical control is proposed to coordinate all those elements of the MG, making the tie-line power flow constant for a period of time, e.g. 15 minutes. Also, a method to calculate the tie-line power flow to be exchanged between the MG and the ADN is explored, and a power ramp rate is given between different dispatch intervals. Finally, a simulation model of the hybrid MG is built and tested. Simulation results show that the proposed hierarchical control strategy can select the proper operational mode and achieve seamless transfer between different modes. It also presents power curtailment functionality when the difference between the WT/PV output power and tie-line exchanged power flow is too large.

Acknowledgement

This work was supported by the Tianjin Science and Technology Support Program Key Project and National Natural Science Foundation of China (15JCZDJC32100, 17JCZDJC31300 and 51577124).
The authors also would like to thank the Danish Energy Technology Development and Demonstration Program (EUDP) and also by the International Science & Technology Cooperation Program of People Republic of China through the Sino-Danish Project Microgrid Technology Research and Demonstration (meter.et.aau.dk).

1. Introduction

The high penetration of wind and solar distributed generation in microgrids (MGs) may cause fluctuations in the tie-line power flow and may affect considerably the electrical distribution system operation. Therefore, large-scale distributed renewable energy generation units have been integrated with energy storage units (ESUs) to form electrical MGs (Yang 2014), (Niknam 2012). At the same time, with the development of concepts like Energy Internet or active distribution networks (ADN), it is expected that more distributed generation (DG) and MGs will be interconnected in the next future (Wang 2015), (Liu 2012), (Haddadian 2017), (Peng 2017), (Zhou 2016). Therefore, in order to facilitate the next ADN's operation, it is necessary to effectively schedule, dispatch, manage, and control MGs or MG aggregators (Fang 2016).

A lot of work has been done in islanded MG control, aiming to balance active power (*P*) and reactive power (*Q*) between generations and loads, thus making MGs to operate as a controlled voltage source. In (Guerrero 2011), (Marzband 2013), (Vandoorn 2013), and (Kim 2014), hierarchical controls of islanded MGs based on droop controlled voltage sources are proposed, which can be interesting when connecting a number of ESUs in an islanded MG. However, in case of grid-connected MGs, the control aim is to make them operate as controlled current sources that should be as much dispatchable as possible. Those MGs are expected to include high level of penetration of renewable resources, such as photovoltaics (PV) and wind turbines (WT), which may lead to severe problems, such as frequency oscillations, voltage instabilities or power line overloading. In order to deal with those problems, it is important to control the power flow of the tie-line that connects each MG to the electrical distribution grid. The tie-line power flow can be controlled by means of different concepts, named: peak-shaving, power ramp-rate limitation, and power smoothing.

The first concept, called **peak shaving**, is shown in Fig. 1(a). It is used in MGs to reduce the need for back-up generators and the large peaks of power delivered to the main grid. An illustrative example can be found in (Shen, 2016), in which a MG energy management strategy with demand response is proposed to provide peak shaving performance. Peak shaving can be performed by using different storage technologies, and can improve demand response, being economically profitable for some technologies (Zheng 2015). Other technologies, such as solar combined cooling and power systems can be also used for peak shaving purposes, but they are limited cases in hot climate areas (Perdichizzi 2015).

The second concept, called **power ramp-rate limitation**, is shown in Fig. 1(b). It consists of limiting the maximum slew-rate of the power caused by the fast variations solar irradiance and wind speed. These

fast slew-rates may affect the stability of the main grid, especially in weak-grid/high-impedance situations (Alam 2014). The effect of cloud-passing in PV systems output power is studied in (Lappalainen 2017), and high power-rates are analyzed, which may affect the grid performance. In this sense, the use of ESUs together with PV/WT is suggested to reduce the maximum power ramp-rate. Some examples about it can be found in La Ola island PV plant, in which the power ramp-rate was measured to be more than 60% of the rated capacity per minute, being desirable to lower it down to 30%. In other cases, it has been lowered down to 50% (Cormode 2013). Furthermore, in networks with high renewable energy penetration like Puerto Rico, authorities have limited the ramp-rates of the PV generators to 10% output power change per minute (Gevorgian 2013).

The third concept called **power smoothing,** shown in Fig. 1(c), makes MGs smoothly integrated into the electrical distribution grid (Lee 2017). This concept consists of smoothing the output power of a DG or MG (Díaz-González 2013). In the literature, several ways to implement power-smoothing can be found. One way is, for instance, to use heat pumps. In (Wang 2014), a regulation method of stabilizing the power fluctuation of MG tie-line by using the heat pump load start/stop is proposed. In another work, (Wang 2015), a coordinated control strategy of a MG by using a combination of a battery and an electric-controlled heat pump load as a virtual-ESU to limit the MG tie-line power fluctuations is proposed. In that work, by setting two different time-constants of two Butterworth filters applied to the virtual-ESU and the battery, the high-frequency and low-frequency components of the MG tie-line power fluctuation are effectively suppressed (Sang 2014), (Wang 2013). Alternatively, in (Liu 2012), the use of composed energy storages to smooth the output power fluctuations of a hybrid PV/WT/ESU MG in different time periods is presented. Further, in (Li 2011), the characteristics and the mathematical models of a hybrid MG are analyzed, and a charge/discharge optimization control of the storage is proposed to smooth the output power fluctuation. Alternatively, in order to reduce the output power fluctuations and to compensate reactive power of a PV/WT/ESU hybrid generation system, an optimal power control combining online rolling-horizon optimization and active real-time control is proposed in (Qi 2014).

However, the aforementioned previous works still present a number of problems such as low-frequency power-flow fluctuations and lack of controllability. In order to solve these problems and to facilitate the management and dispatch of the future distribution grid, this paper proposes a concept called **flat tie-line power scheduling**, shown in Fig. 1(d). It consists on controlling every MG to act as generator/load, thus maintaining the tie-line power flow as constant/flat as possible during a determined period of time. This concept is also able to integrate the previous ones, i.e. peak shaving, power ramp-rate limitation, and power smoothing. A comparison between these state-of-the-art concepts and the proposed flat tie-line power scheduling concept, in relation with the needed qualitative size of the storage, is shown in Table I. By using the proposed concept, a hybrid MG, including PV, WT and ESUs, can be controlled in a hierarchical way to coordinate all those elements making the tie-line power flow constant for a period of time, e.g. 15 minutes. This way, MGs can make full use of the generated renewable energy, while facilitating their dispatch and management when integrating them in future ADNs.

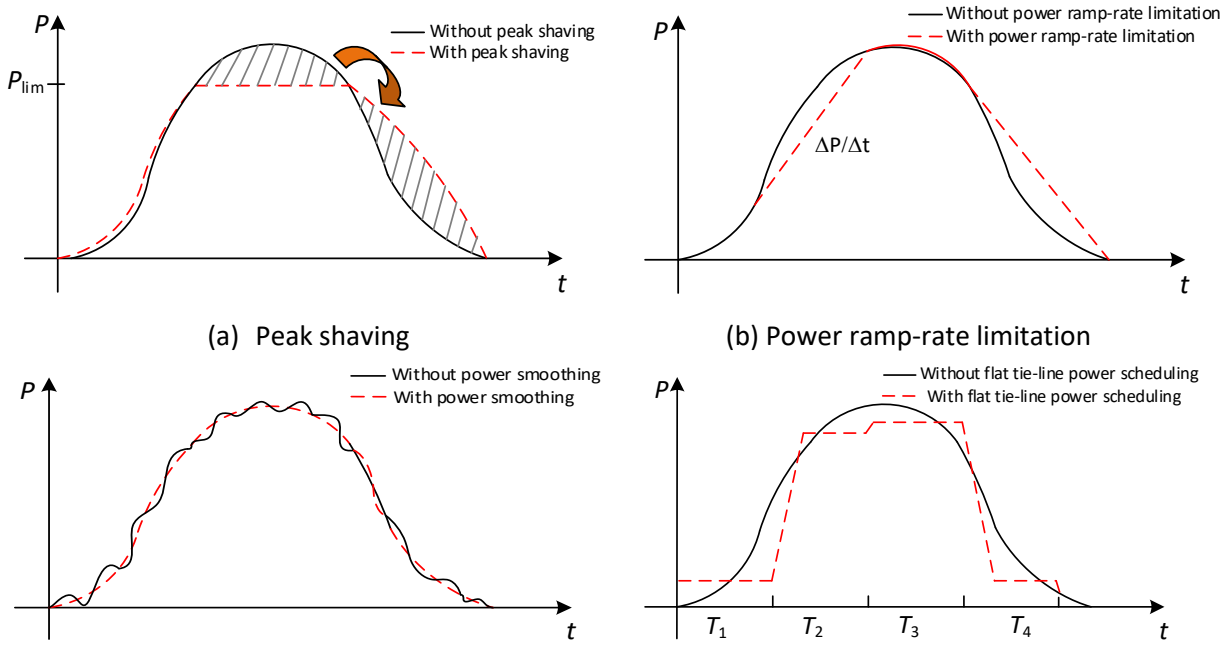

Fig. 1. Tie-line power flow control methods.

Table I. Comparison between peak-shaving, power ramp-rate limitation, power smoothing concepts and the proposed flat power scheduling.

Method	***Function***	***Storage Capacity***
Peak shaving	Reduce the utility peak power by using local energy storage and/or additional generators	Large
Power ramp-rate limitation	Limit the power slew-rate by adding inertia through storage	Small
Power smoothing	Smooth short-term fluctuations by adding energy storage	Small/None
Flat power scheduling	Support power/energy to schedule flat power during a time to facilitate the management in an ADN	Medium

A method to calculate the tie-line power flow to be exchanged between the MG and the AND is presented, and a power ramp rate is given between different dispatch intervals. Then, the structure of a hybrid PV/WT/ESU MG is introduced. In this power architecture, the battery is directly connected to the PV side through a DC/DC converter, thus reducing the number of conversions, and the PV power-voltage output characteristic is used to implement the maximum power point tracking (MPPT) control. The proposed hierarchical coordination control takes into account the actual operating conditions, such as the wind speed curve, the instantaneous irradiance conditions, and the storage capacity limit. The proposed

method has been implemented and simulated for different operation conditions, showing the seamless transition between the different operation states.

The paper is organized as follows. Section II describes the hybrid MG power architecture. Section III presents a method to calculate the tie-line constant power for a period of time, a power ramp rate between different dispatch times, and all possible operation states. The WT back-to-back converters controllers, variable pitch angle control of the WT, the active and reactive power controllers of the PV-inverter, and the battery DC/DC charge/discharge controller are presented in section IV. Section V presents the system parameters and simulation results. Finally, Section VI summarizes this paper.

2. Microgrid System Architecture

Fig. 2 shows the block diagram of *n* MGs connected to an ADN through tie-lines. Each MG (MG1, MG2,…MGn) contains a number of local controllers for each element (e.g. PV, WT, ESU) and central controller that manage the whole MG. Note that every MG has a scheduled flat tie-line power reference, which is desirable to be constant during certain period (T_1, T_2, T_3…) in order to facilitate the dispatch and management of the future ADNs. The scheduled tie-line often comes from the average value of the predicted total MG available power, which is however out of the scope of this paper (Liu 2014).

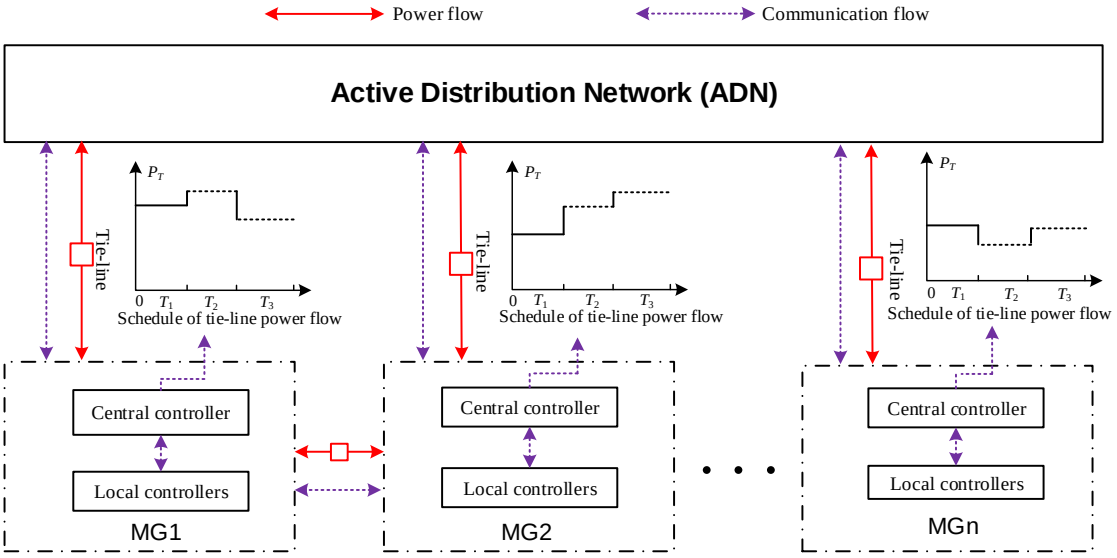

Fig. 2. Integration of microgrids in the active distribution network (ADN).

Fig. 3 shows the block diagram of a hybrid MG, including power stages and control systems. The MG includes a small WT unit, a PV system, and a battery-based ESU. The small WT unit comprises a variable speed gearbox, a doubly-fed induction generator (DFIG), and a back-to-back converter connected to the rotor side. The PV system is connected to the DC bus by an anti-reverse diode, while the battery is connected by the bidirectional DC/DC converter to the same bus. The inverter is connected to the AC bus through a Δ-Y step-up transformer. Finally, the hybrid MG is connected to the distribution network by a step-up transformer. Notice that PV array does not require a dedicated DC/DC converter, being the ESU DC/DC converter responsible for the MPPT functionality and ESU management at the same time. Thus, this architecture presents higher efficiency than using two separate DC/DC converters.

The control system includes a central controller and a set of local controllers. The central controller includes a MG energy management system (EMS), which is responsible for wind speed, load behavior, and solar radiation forecasting. It also includes tie-line active and reactive power (P/Q) calculation, selection and switching of the operation modes, reference value calculation to be sent to the local controllers, selection of battery charge/discharge modes, and battery management.

The coordinated control between WT, PV and ESU inside the MG is designed to meet the dispatch requirements of the ADN, and to achieve constant power inside a range of time. The local controllers include MPPT, variable pitch control of wind generation, PV-inverter P/Q control, battery charge/discharge controllers, constant DC bus voltage, and voltage/current control loops.

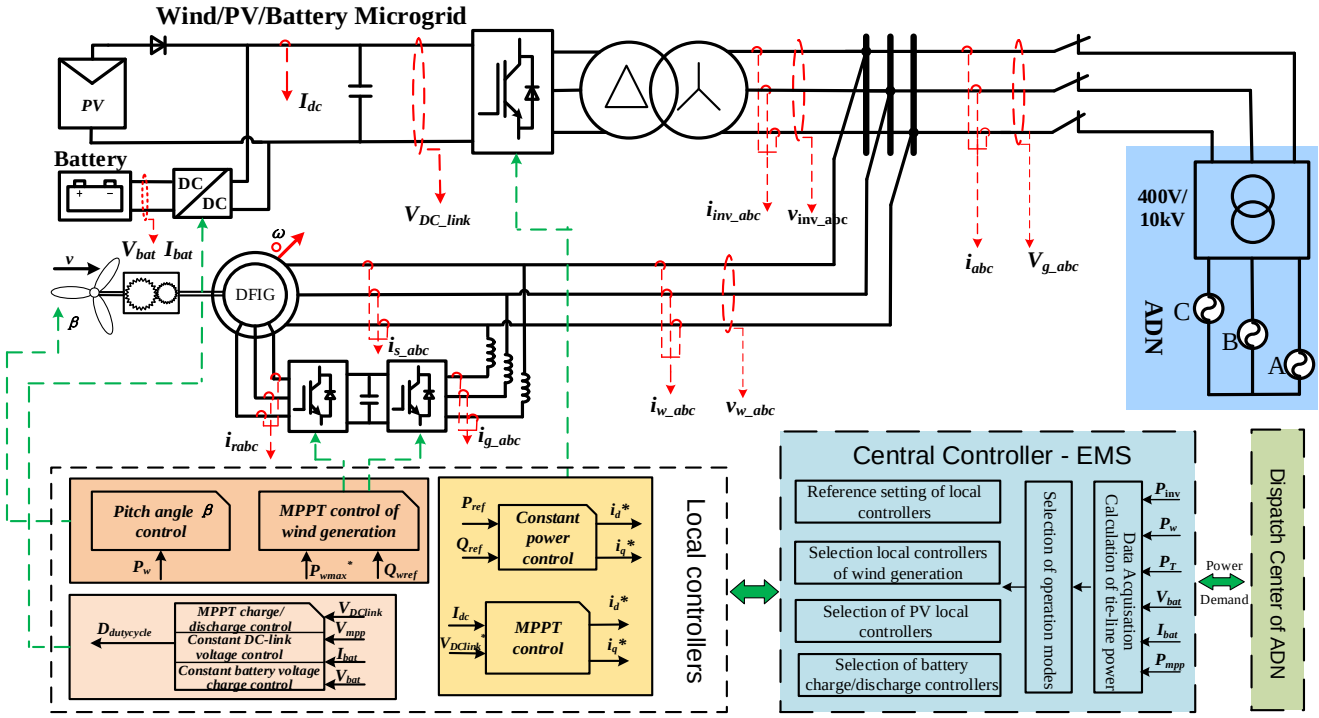

Fig. 3. Structure of hybrid microgrid.

3. Central Controller

Back to Fig. 3, the control architecture of the hybrid MG is split in two main types of controllers: the central controller, which is connected to the dispatch center of the ADN, and a number of local controllers connected as well to the central control. The central controller consists of the data acquisition of a number of variables, such as P_{inv}, P_W, P_T, V_{bat}, I_{bat}, and P_{MPP}. With this data acquisition, it is able to calculate the tie-line power and to select between operation modes.

3.1 Calculation of the tie-line power reference

The tie-line power reference can be calculated to be constant in a time period, here 15 minutes, by using the energy balance method. By neglecting the line impedance power losses, the total output power P_{gl} of the WT/PV/ESU hybrid MG at any time can be expressed as follows,

$$P_{gl} = P_W + P_{PV} + P_B \qquad (1)$$

where P_W, P_{PV}, and P_B are the active power of WT, PV, and battery-based ESU, respectively. When the battery is discharging, P_B is positive, while when it is charging, P_B is negative.

Assuming that the predicted wind speed and the irradiation during the dispatching period T are known, it is possible to calculate the electric energy generated by the WT and the PV during T as W_w and W_{pV}, shown as follows

$$W_W + W_{PV} = \int_0^T P_W \, dt + \int_0^T P_{PV} \, dt. \qquad (2)$$

The average power P_T during T can be calculated as

$$P_T = \frac{W_w + W_{PV}}{T}. \qquad (3)$$

Therefore, the output active power reference during the dispatching period T (P_T^*) cannot be surpassed by the output power averaged over T (P_T), which should be ideally equal, that is $P_T^* = P_T$. To the best knowledge of the authors, there is no standard to select the power ramp rate in distribution electrical networks. However, by observing the good practices, if MG acts as a load from the viewpoint of the distribution network, the ramp-rate should not be too high. Here, we select the power ramp-rate as 30% of the rated power per minute between different dispatch intervals, as a good compromise between fast response and stability.

The battery capacity is selected by using the energy and power balance methods in order to smooth the MG output power. On the one hand, the energy balance is usually ensured by calculating the energy produced by the generators or consumed by the critical loads of the MG during a certain period of time, and the battery capacity is equal to the generated or consumed energy. On the other hand, the power balance method generally analyzes the maximum difference between the generated and consumed powers, the highest peak to determine battery charge current, and the lowest valley to determine the battery discharge current.

3.2 Operation Modes

In order to ensure proper behavior of the MG, a number of operation modes and power flow of the WT/PV/ESU hybrid MG are determined by the state machine presented in Fig. 4. The two-stage battery charge technique is employed as follows (Chen 2012):

- **Stage 1.** A limited current charge is used if V_{bat} is lower than the threshold voltage (V_{th}). Notice that V_{th}=400V corresponds to a state of charge (SoC) about 86 %, which is near to the maximum battery terminals voltage.
- **Stage 2.** A constant voltage charge is used if V_{bat} is higher or equal to V_{th}.

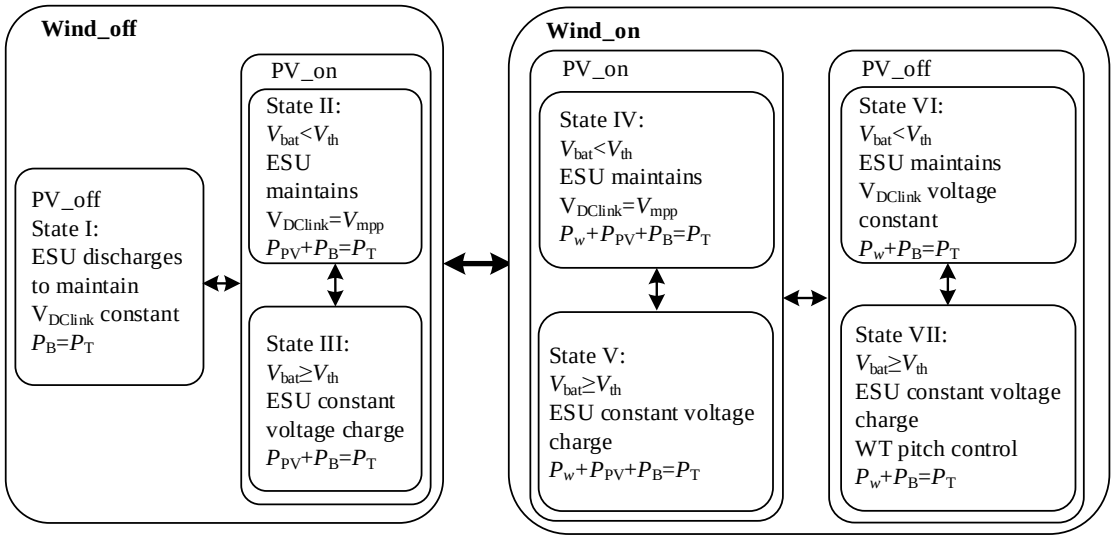

Fig. 4. Operation states of the hybrid microgrid.

The different operation states are defined according to Fig. 5 as follows:

- **State I:** No wind power (wind speed outside the operational ranges) and no PV generation are available. The ESU produces the needed power P_B to maintain the DC-link voltage constant, thus P_T=P_B.
- **State II:** No wind power available. The ESU voltage is below V_{th}, so that the ESU keeps the DC-link voltage following V_{mpp}, in order to make the PV array operate at the maximum power operation point. The ESU power flow is bidirectional, so that it can make the PV output power following the scheduled output power P_T^*. This way, both PV and ESU contributes to the required $P_T = P_{PV} + P_B$
- **State III:** No wind power available. The voltage of the ESU is higher than V_{th}, so that the ESU is operating at constant voltage to avoid its overcharge. Thus the PV array may operate out of the maximum operating point in a power curtailment fashion.
- **State IV:** Wind and solar power are available. The ESU voltage is below V_{th}, so that the ESU keeps DC-link voltage following V_{mpp}, or eventually making the PV array operating out of the maximum power operation point. This is automatically achieved to maintain the required P_T, and since the WT pitch control is relatively slow, it is faster to adjust the PV operation point. This way, WT, PV and ESU contributes to the required $P_T = P_W + P_{PV} + P_B$
- **State V:** Wind and solar power are available. The voltage of the ESU is higher than V_{th}, so that the ESU is operating at constant voltage to avoid its overcharge. Thus, the PV array may operate inside or outside the maximum operating point, while the WT may operate at that point all the time.
- **State VI:** Wind power is available, but solar power is not. The voltage of the ESU is below V_{th}, so that the ESU maintains the DC-link voltage constant, while the WT may operate at the maximum power operation point. As the power flow of ESU is bidirectional, it can be either charged or discharged. This way, both WT and ESU contribute to the required $P_T = P_W + P_B$
- **State VII:** Wind power is available, but solar power is not. The ESU voltage is higher than V_{th}, so that the ESU is operating at constant voltage to avoid its overcharge. Thus the WT may operate outside of the maximum operating point by using its pitch control.

Note that during states III, IV and V, ESU reaches the maximum charging current, which may cause the PV to operate out of the maximum operating point automatically. A scenario in which the ESU SoC is too low to smooth the PV and/or WT output powers is not considered here. The reason of this is that ESU mainly provides power support during each dispatching time, i.e. 15 minutes. Nevertheless, if we properly size the battery capacity, this situation will not happen. In Table II the transition conditions between states are presented, being P_{mpp} the maximum output power of PV. Notice that WT should operate inside the allowable wind speed range; otherwise it may stop if the wind speed is lower than the minimum speed v_{min} or higher than the maximum speed v_{max}.

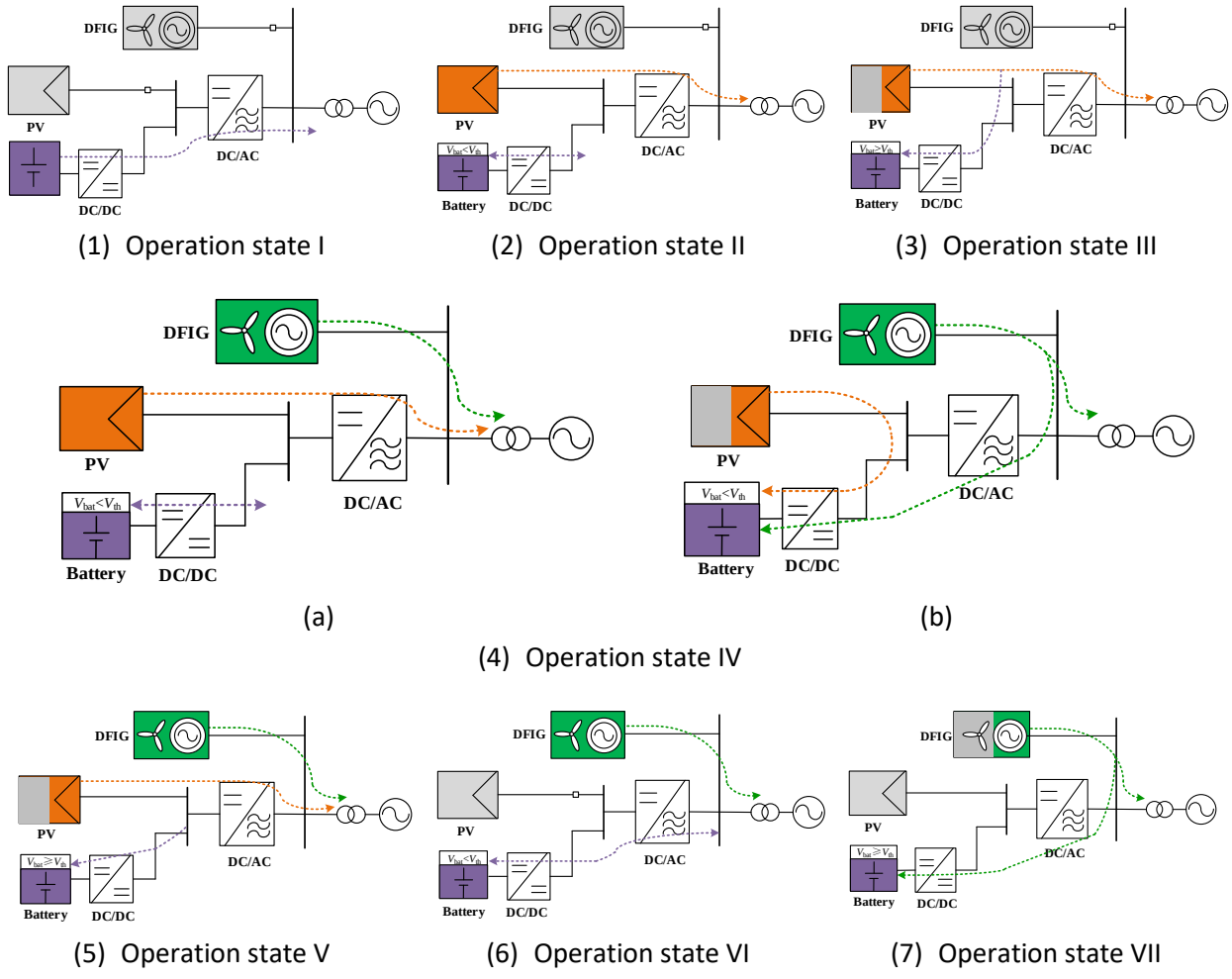

Fig. 5. Operation states of the hybrid MG

Table II. Conditions of the operation states

State	***Condition***
I	(P_{mpp}=0)& ($v<v_{min}$ || $v>v_{max}$)
II	(P_{mpp}>0)& ($v<v_{min}$ || $v>v_{max}$)&($V_{bat}<V_{th}$)
III	(P_{mpp}>0) & ($v<v_{min}$ || $v>v_{max}$) & ($V_{bat}\geq V_{th}$)

IV	(P_{mpp}>0) & ($v_{max}\geq v\geq v_{min}$)&($V_{bat}<V_{th}$)
V	(P_{mpp}>0) & ($v_{max}\geq v\geq v_{min}$)&($V_{bat}\geqslant V_{th}$)
VI	(P_{mpp}=0) & ($v_{max}\geq v\geq v_{min}$)&($V_{bat}<V_{th}$)
VII	(P_{mpp}=0) &($v_{max}\geq v\geq v_{min}$)&($V_{bat}\geqslant V_{th}$)

4. Local Controllers

4.1 Wind turbine and DFIG Control

The WT unit is a variable speed constant frequency system, including DFIG and turbine with an additional variable pitch angle. The local controllers of WT unit include the MPPT and the pitch angle control (He 2012).

When the wind speed is lower than the maximum speed v_{max}, the WT unit should output its maximum power P_{wmax}^* at a certain wind speed v, thus being operated with a DFIG rotor-side controller, as shown in Fig. 6(a), which includes a PLL to synchronize with the slip angle. A double-loop control is used in the DFIG rotor-side converter, where the outer loop is a power controller with a maximum power reference P_{wmax}^* at a certain wind speed calculated by a standard MPPT algorithm, and an inner current loop. The control aims to maximize the wind energy utilization. The DFIG grid-side controller is shown in Fig. 6 (b), which is used to decouple rotor and the grid sides by regulating the capacitor voltage of the back-to-back converter and a current control loop operating at the grid AC voltage stationary reference frame (Song 2010).

On the other hand, the pitch angle control, shown in Fig. 6(c), is used to limit the output power of the WT unit by regulating the pitch angle β. By comparing the measured output power P_w of the WT and the reference power P_w^*, the error enters the pitch actuator through the PI controller to produce the required pitch angle reference β^*, and the turbine pitch angle changes accordingly in order to make the output power P_w as P_w^*. Notice that the pitch actuator is usually simplified as a first order system, where K_β is a proportional coefficient, and τ_β is the time constant of the pitch actuator.

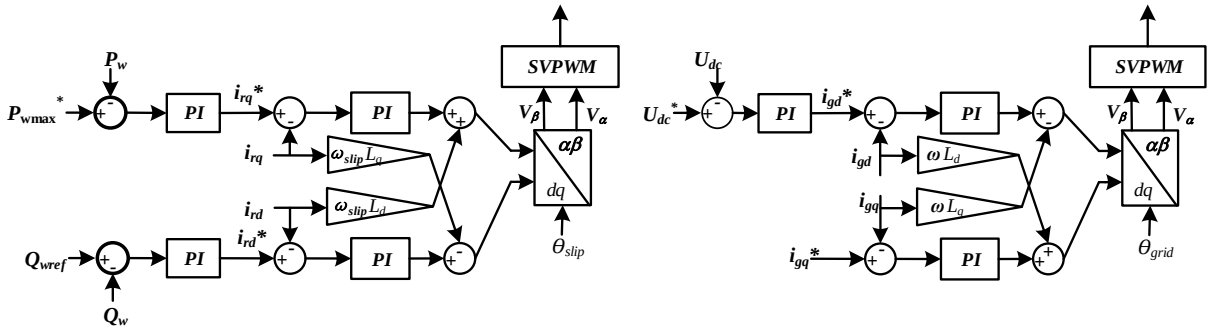

(a) DFIG rotor-side controller

(b) DFIG grid-side controller

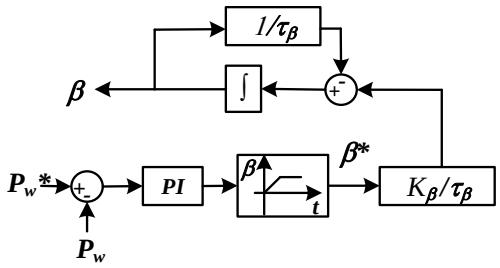

(c) Pitch control

Fig. 6. Local controllers of the WT unit

4.2 PV Inverter Control

Fig. 7(a) shows the power-to-voltage characteristic of a PV array. Notice that although the controller tries to get the maximum power point (MPP) in ideal conditions, however, in some occasions the operation point may go outside the MPP thus shifting it to the right side towards the open circuit voltage (V_{OC}), as mentioned in section 3.2.

Then, a P/Q controller using the synchronous reference frame, i.e. *dq*-transformation, is used for the PV inverter, as shown in Fig. 7(b), which includes a PLL to synchronize the converter with the distribution grid voltage, a power and a current control loops. The control aims at achieving the output active and reactive powers of the PV-inverter to be equal to the reference power (Xiao 2015), according to: $P_{REF} = P_T^* - P_W$ and $Q_{REF} = 0$.

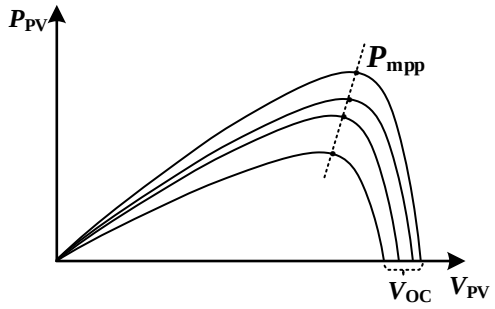

(a) P-V characteristic

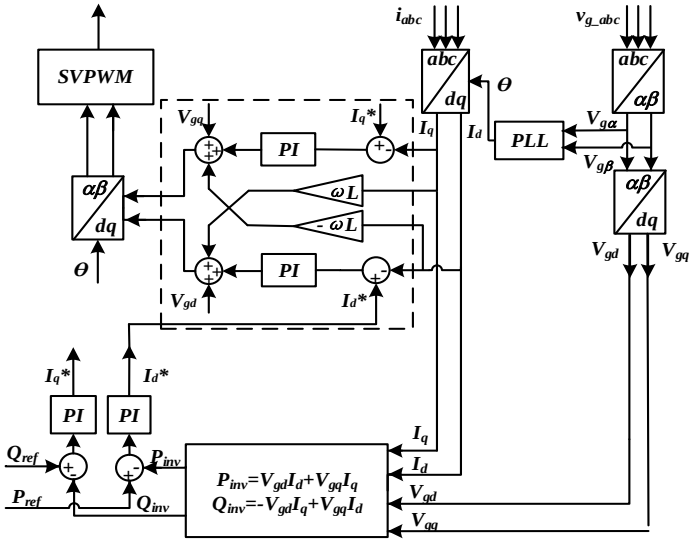

(b) P/Q controller of the PV inverter

Fig. 7. PV characteristic and inverter control.

4.3 Battery charge/discharge control

The battery charger consists of a bi-directional DC/DC converter, acting as a buck configuration for charging or a boost for discharging the battery. The battery controller is shown in Fig. 8, where V_{bat} is the

voltage at the terminals of the battery, V_{bat}* *is the voltage reference,* I_{bat} is the battery output current, V_{DClink} is the DC bus voltage of the PV system, and $D_{dutycycle}$ is the duty cycle of the DC/DC converter. The controller has two operation modes, as can be seen in Fig. 8.

The first one is the limited current control, which corresponds to $V_{bat}<V_{th}$, and it consists of two control loops: voltage and current loop. The outer voltage loop aims at achieving MPPT or curtailing PV output power, while the inner current loop aims at charging/discharging the battery according to the sign of I_{bat}. When the solar irradiation is low or need to limit the PV output power, a higher DC voltage is maintained in order to disable PV generation. Note that I^*_{bat} is limited by a saturation bounded by I_{Cmin} = -0.2C and I_{Dmax} = +1C in order to limit the charge/discharge currents. This is a recommendation from the battery manufacturer, which can be adjusted according to the battery technology to be used.

The second is the constant voltage control, which corresponds to $V_{bat}\geq V_{th}$, and it consists of a voltage and a current loop. The voltage loop is to regulate the battery voltage (V_{bat}), while the current loop is the same as used in the first operation mode. Notice that V_{bat}^* is set as V_{th}, so that is equal to 400V.

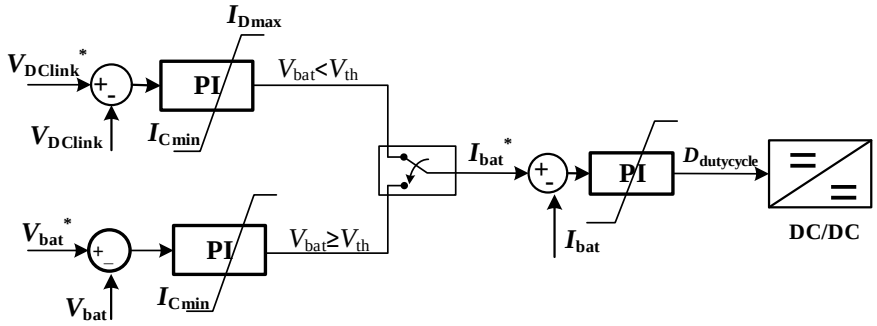

Fig. 8. Battery DC/DC converter controller

5. Simulation Case-Study of WT/PV/ESU Hybrid MG

The simulation model of a WT/PV/ESU hybrid MG is implemented in Matlab/Simulink SimPowerSystems toolbox. The central controller is implemented using Simulink/Stateflow. The main parameters of the system are shown in Table III, including DFIG, its back-to-back grid-side and rotor-side converter controllers, PV inverter, DC/DC converter controller, and battery parameters (He 2012), (Xiao 2015). The selected battery is a lead-acid battery with the parameters listed in Table III and the model can be found in (Kim 2011).

Table III. Parameters of WT/PV/ESU hybrid MG

Parameters of DFIG	Value
Rated power /kVA	250
Rated voltage /V	400
Rated speed rev/min	1800
Number of poles	2
Stator and rotor resistor /Ω	0.02, 0.02

Stator and rotor inductor /Ω	0.0044, 0.0044
Excitation inductor /Ω	0.0042
Inertia (J) /kg·m^2	250
Parameters of grid-side converter	**Value**
Line inductor /mH	1
DC side capacitor /mF	15
DC bus voltage /V	810
Gains of inner loop controller k_{p1}, k_{i1}	15, 30
Gains of outer loop controller k_{p2}, k_{i2}	3, 30
Parameters of rotor-side converter	**Value**
Rated power of rotor-side converter /kVA	75
Gains of active current inner loop k_{p1}, k_{i1}	25, 1
Gains of reactive current inner loop k_{p2}, k_{i2}	40, 9
Gains of active power outer loop k_{p3}, k_{i3}	0.0032, 0.059
Gains of reactive power outer loop k_{p4}, k_{i4}	0.0029, 0.025
Parameters of the lead-acid battery	**Value**
Rated voltage of battery /V	384
Battery capacity /Ah	800
Maximum charge current /A	160
Maximum discharge current /A	800
Parameters of DC/DC converter	**Value**
Voltage loop gains of limited current control k_{p1}, k_{i1}	9, 50
Voltage loop gains of constant voltage control k_{p2}, k_{i2}	9, 50
Inner current control loop gains k_{p3}, k_{i3}	0.9, 10
Parameters of the PV inverter	**Value**
Rated power of PV inverter /kVA	100
Capacity of Δ-Y step-up transformer /kVA	150
Ratio of Δ-Y step-up transformer	300/400
Filter inductor /mH	2
Filter resistor /Ω	0.002
DC voltage controller gains k_{p1}, k_{i1}	1.2, 35
Active power outer loop gains of PQ control k_{p2}, k_{i2}	0.003, 0.9
Reactive power outer loop gains of PQ control k_{p3}, k_{i3}	0.003, 1.5
Current inner loop gains of PQ control k_{p4}, k_{i4}	21, 440

The simulations are based on the average model of the power electronics converters (Vasquez 2013). Furthermore, in order to perform the simulations within a reasonable time, the data were time-scaled considering that 10s corresponds to 1s of simulation. Thus, the real battery capacity is divided by ten as well (Luna 2016). Meteorological real data including wind speed and solar irrandiance was provided by

the Photovoltaic Research Program of Aalborg University, Denmark (Aalborg 2017), which has been used to test the system for a period of 1800s.

Fig. 9 shows the wind speed profile, which remains between 6 m/s and 14 m/s, although occasionally at 570s goes below those values. Fig. 10 shows the solar irrandiance curve with values between 800 and 1,000 W/m2 which may go down to 200-300 m/s due to the passing clouds effect.

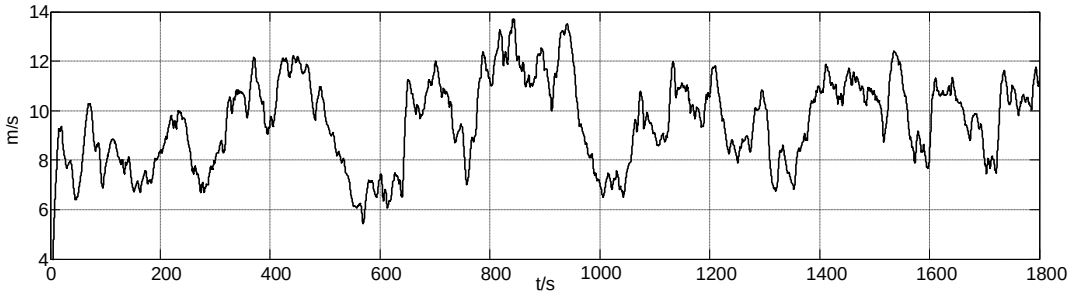

Fig. 9. Wind speed (time scale 10:1s)

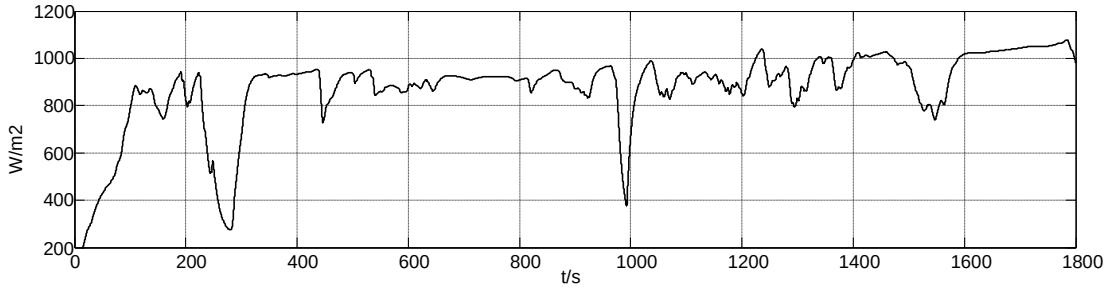

Fig. 10. Solar irradiance curve (time scale 10:1s)

Note that the DFIG wind turbine cut-in wind speed is 6m/s, the rated wind speed is 10.5m/s, and the cut-out speed is 20m/s. In addition, the selected lead-acid batteries present a capacity of 800 Ah, rated voltage of 384 V, maximum charging current 160A, and minimum discharging SoC of 20%.

Fig. 11 shows the active power flow from the MG to the distribution electrical grid (P_T^*) in contrast to its reference (P_T), which is changing from 220 kW to 250 kW at 90 s, with a power ramp-rate of 30% of the rated power per minute. Note the good power tracking presented by the MG system. Figs. 12, 13 and 14 show the DFIG rotor, stator and total wind power generation (P_r, P_s, and P_w). Notice that, at the time 57 s, there is a fast power change due to the low speed wind that makes the WT almost to stop. Fig. 15 shows the PV maximum power reference (P_{mpp}) and the actual PV power generation (P_{PV}). When the battery reaches the current limit, PV power is curtailed, and the PV voltage operation point moves outside the MPP, as can be seen in Fig. 16. The PV dc-link voltage is ranged between V_{mpp} and V_{oc}, according to Fig. 7(a). In this application this range is about 500V - 650V.

Note that the power curtailment periods coincide with those in which the battery is absorbing its maximum power (-60 kW, i.e. -160 A), as can be observed in Fig. 17. Fig. 18 shows the tracking performance of the PV inverter output power (P_{inv}), when following the power reference P_{REF}. Notice the good accuracy performed by the P/Q controller. Reactive power in the tie-line, not shown here was always

settled at zero. The evolution of the battery SoC can be observed in Fig. 19. The SoC value is estimated in simulation model for simplicity by using the well-known coulomb counting model, which can be obtain as follows (Kim 2011):

$$SoC(t) = SoC(0) - \frac{1}{C}\int I_{bat}(t)\,dt \qquad (4)$$

where SoC(0) is the initial SoC of the battery, and C the usable capacity of the battery. It is worth notice that this technique can be improved by considering efficiency, nonlinearities, and so on, which is out of the scope of this paper. The estimated error of the SoC coulomb counting method for the lead-acid batteries is maximum 6% for each cycle (Ng 2009) when correction factors are included and 14% without. The error is reset every cycle, once the SoC battery reaches 100%. Notice that here the SoC is only used for monitoring purposes, so that it does not affect the control system accuracy. The proposed algorithms use V_{bat} instead of SoC to switch among controllers.

Figs. 20 and 21 show the battery voltage and current (V_{bat}, and I_{bat}). When the charge current reaches the maximum (160 A), the battery is being charged with a constant power (60 kW), and the battery voltage almost does not increase. Fig. 22 shows the inverter output current and Fig. 23 shows the output current of the WT. Both currents are decomposed in *d* and *q* components, being *q*-component zero due to the absence of reactive power. Since the distribution grid voltage is stiff, *d*-component current waveforms are following their corresponding output power waveforms.

The different operation modes can be observed in Table IV, including the time period, the operation modes of WT/PV generators (disabled, MPPT, or limited, i.e. power curtailment), ESU modes (charging/discharging), PV inverter active power reference (P_{inv}), tie-line power (P_T), and the operation state number.

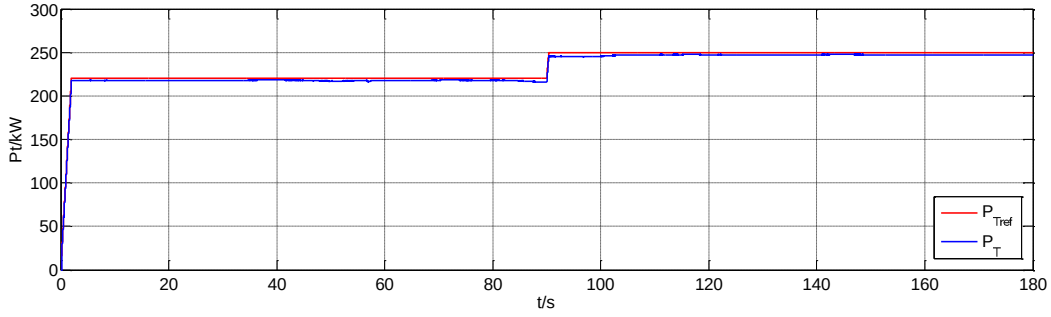

Fig. 11. Reference and actual tie-line active power (P_T^* & P_T)

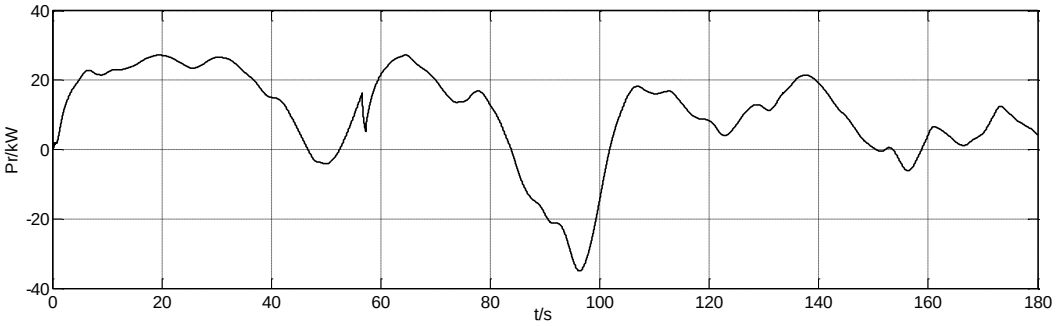

Fig. 12. Output active power of the DFIG rotor (P_r)

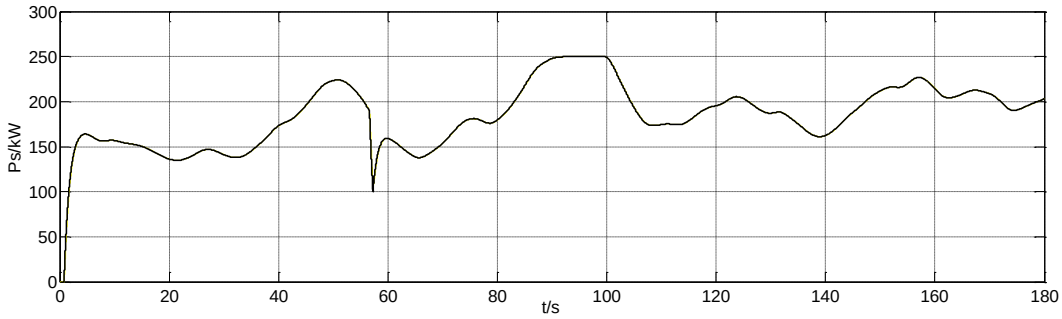

Fig. 13. Active power of the DFIG stator (P_s)

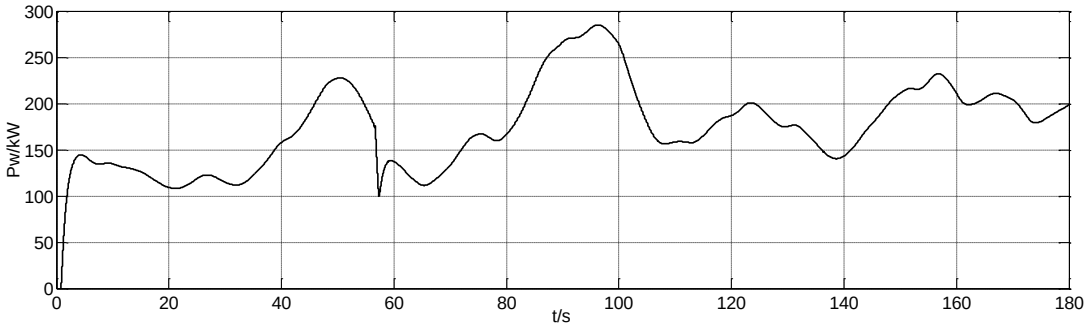

Fig. 14. Wind power generation (P_w=P_r+P_s)

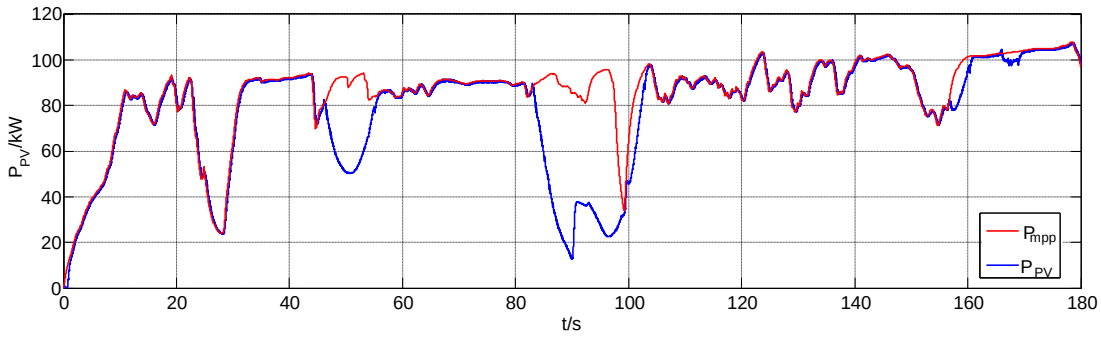

Fig. 15. PV maximum power reference (P_{mpp}) and actual PV power generation (P_{PV})

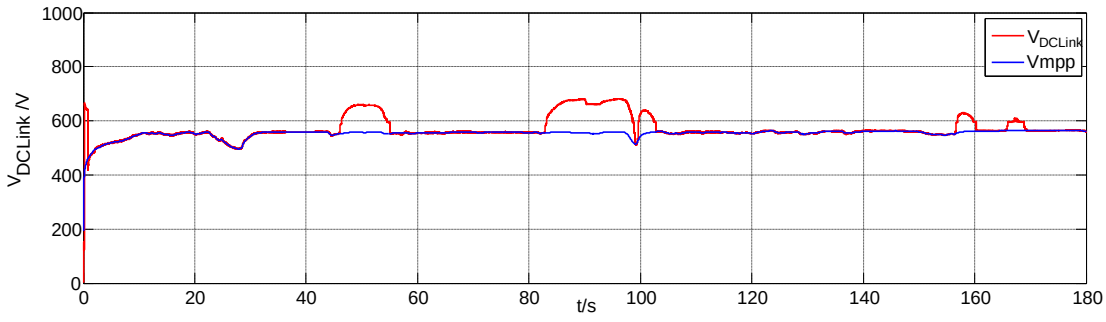

Fig. 16. PV maximum-power voltage reference (V_{mpp}) PV and actual DC-link voltage (V_{DCLink})

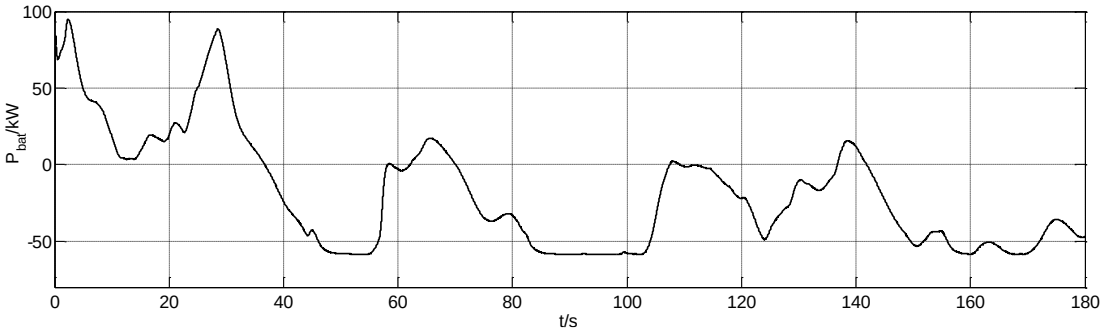

Fig. 17. Battery output power (P_B)

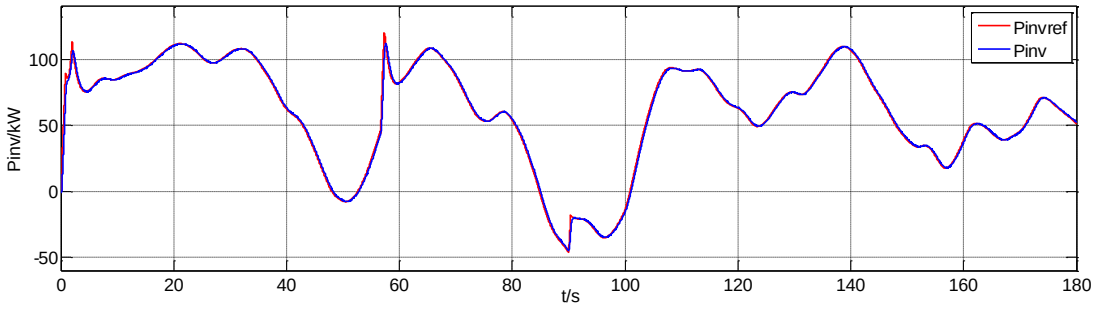

Fig. 18. Reference and output power of the PV inverter (P_{inv}=P_B+P_{PV})

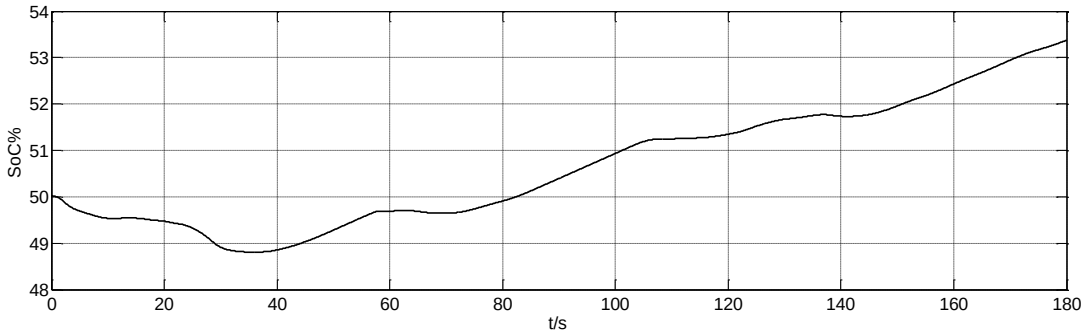

Fig. 19. SoC of the Battery

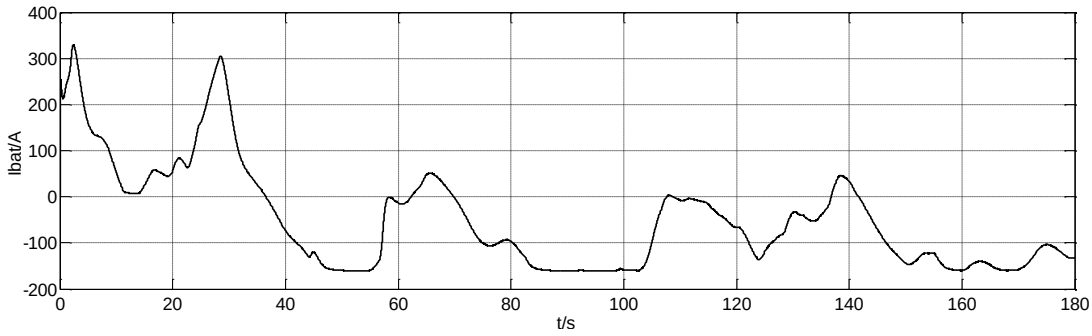

Fig. 20. Battery current

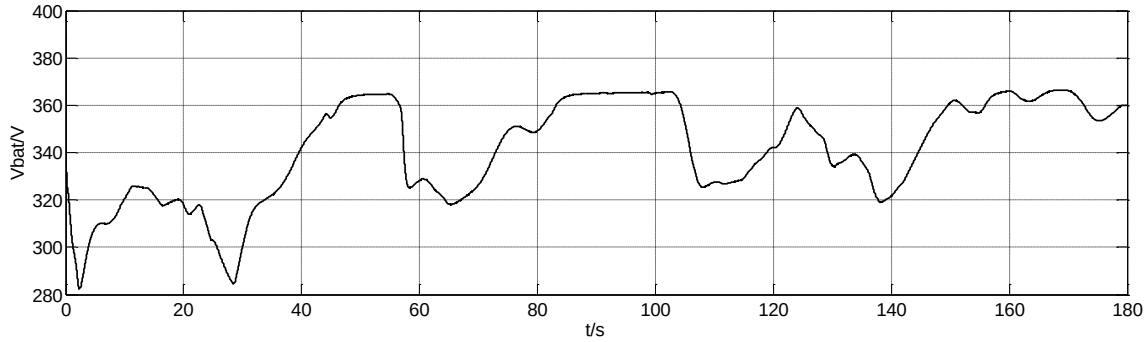

Fig.21. Battery voltage

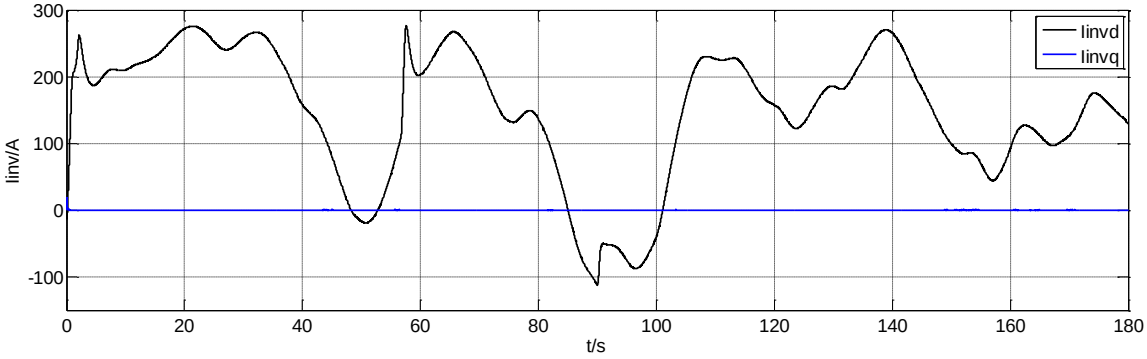

Fig.22. Inverter d-q current

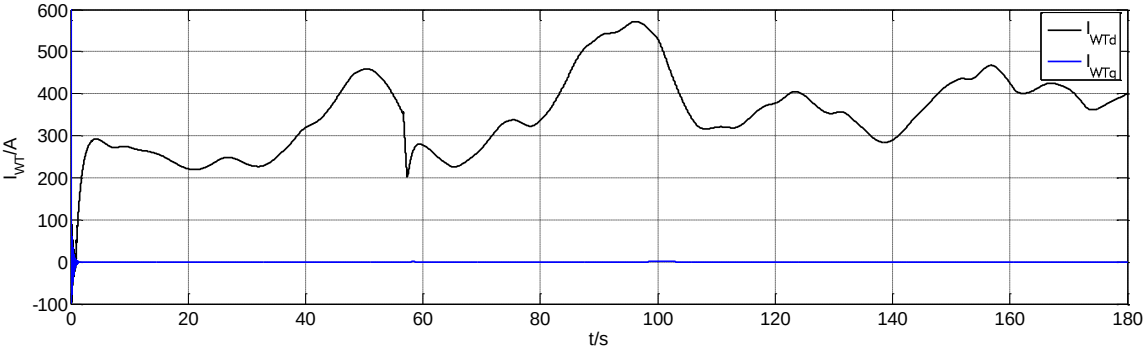

Fig.23. WT d-q current

Table IV. The operation state of WT/PV/ESU hybrid MG

Simulation time (s)	WT	PV	ESU	PV-inverter power reference	Tie-line power	Operation state
0.1-0.7	disabled	disabled	discharge	$P_{\mathrm{ref}} = P_{\mathrm{T}}$	$P_{\mathrm{T}} = P_{\mathrm{B}}$	I
0.7-0.9	disabled	MPPT	discharge	$P_{\mathrm{ref}} = P_{\mathrm{T}}$	$P_{\mathrm{T}} = P_{\mathrm{PV}} + P_{\mathrm{B}}$	II
0.9-37	MPPT	MPPT	discharge	$P_{\mathrm{ref}} = P_{\mathrm{T}} - P_{\mathrm{w}}$	$P_{\mathrm{T}} = P_{\mathrm{W}} + P_{\mathrm{PV}} + P_{\mathrm{B}}$	IV
37-45	MPPT	MPPT	charge	$P_{\mathrm{ref}} = P_{\mathrm{T}} - P_{\mathrm{w}}$	$P_{\mathrm{T}} = P_{\mathrm{W}} + P_{\mathrm{PV}} - P_{\mathrm{B}}$	IV
45-55	MPPT	limited	charge	$P_{\mathrm{ref}} = P_{\mathrm{T}} - P_{\mathrm{w}}$	$P_{\mathrm{T}} = P_{\mathrm{W}} + P_{\mathrm{PV}} - P_{\mathrm{B}}$	IV
55-62	MPPT	MPPT	charge	$P_{\mathrm{ref}} = P_{\mathrm{T}} - P_{\mathrm{w}}$	$P_{\mathrm{T}} = P_{\mathrm{W}} + P_{\mathrm{PV}} - P_{\mathrm{B}}$	IV

62-70	MPPT	MPPT	discharge	$P_{\mathrm{ref}} = P_{\mathrm{T}} - P_{\mathrm{w}}$	$P_{\mathrm{T}} = P_{\mathrm{W}} + P_{\mathrm{PV}} + P_{\mathrm{B}}$	IV
70-83	MPPT	MPPT	charge	$P_{\mathrm{ref}} = P_{\mathrm{T}} - P_{\mathrm{w}}$	$P_{\mathrm{T}} = P_{\mathrm{W}} + P_{\mathrm{PV}} - P_{\mathrm{B}}$	IV
83-90	MPPT	limited	charge	$P_{\mathrm{ref}} = P_{\mathrm{T}} - P_{\mathrm{w}}$	$P_{\mathrm{T}} = P_{\mathrm{W}} + P_{\mathrm{PV}} - P_{\mathrm{B}}$	IV
90-100	limited	limited	charge	$P_{\mathrm{ref}} = P_{\mathrm{T}} - P_{\mathrm{w}}$	$P_{\mathrm{T}} = P_{\mathrm{W}} + P_{\mathrm{PV}} - P_{\mathrm{B}}$	IV
100-103	MPPT	limited	charge	$P_{\mathrm{ref}} = P_{\mathrm{T}} - P_{\mathrm{w}}$	$P_{\mathrm{T}} = P_{\mathrm{W}} + P_{\mathrm{PV}} - P_{\mathrm{B}}$	IV
103-137	MPPT	MPPT	charge	$P_{\mathrm{ref}} = P_{\mathrm{T}} - P_{\mathrm{w}}$	$P_{\mathrm{T}} = P_{\mathrm{W}} + P_{\mathrm{PV}} - P_{\mathrm{B}}$	IV
137-142	MPPT	MPPT	discharge	$P_{\mathrm{ref}} = P_{\mathrm{T}} - P_{\mathrm{w}}$	$P_{\mathrm{T}} = P_{\mathrm{W}} + P_{\mathrm{PV}} + P_{\mathrm{B}}$	IV
142-157	MPPT	MPPT	charge	$P_{\mathrm{ref}} = P_{\mathrm{T}} - P_{\mathrm{w}}$	$P_{\mathrm{T}} = P_{\mathrm{W}} + P_{\mathrm{PV}} - P_{\mathrm{B}}$	IV
157-160	MPPT	limited	charge	$P_{\mathrm{ref}} = P_{\mathrm{T}} - P_{\mathrm{w}}$	$P_{\mathrm{T}} = P_{\mathrm{W}} + P_{\mathrm{PV}} - P_{\mathrm{B}}$	IV
160-165	MPPT	MPPT	charge	$P_{\mathrm{ref}} = P_{\mathrm{T}} - P_{\mathrm{w}}$	$P_{\mathrm{T}} = P_{\mathrm{W}} + P_{\mathrm{PV}} - P_{\mathrm{B}}$	IV
165-167	MPPT	limited	charge	$P_{\mathrm{ref}} = P_{\mathrm{T}} - P_{\mathrm{w}}$	$P_{\mathrm{T}} = P_{\mathrm{W}} + P_{\mathrm{PV}} - P_{\mathrm{B}}$	IV
167-180	MPPT	MPPT	charge	$P_{\mathrm{ref}} = P_{\mathrm{T}} - P_{\mathrm{w}}$	$P_{\mathrm{T}} = P_{\mathrm{W}} + P_{\mathrm{PV}} - P_{\mathrm{B}}$	IV

5. Conclusion

In this paper, the concept of flat tie-line power scheduling is proposed. Based on that, a control architecture to coordinate the power generation of a small WT and a PV array of a grid-connected MG supported by a battery-based ESU, is developed. The MG control system is able to ensure flat output power, regarding the power availability of the WT/PV resources and ADN scheduling, thus determining its operation state. The central controller send the proper commands to the local controllers in order to determine the local power references of the renewable energy resources, and to select the proper operational mode of the ESU. The control architecture presents the following features:

- Makes the MG be seen as single dispatchable entity from the ADN viewpoint.
- Achieves predetermined power ramp-rate when changing its power reference.
- Selects proper operation modes, and achieves seamless transfer between them at the same time.
- Performs power curtailment functionalities in case of the difference between the WT/PV output power and tie-line exchange power flow is too large to be supported by the ESS.
- Ensures power injected into the grid to be constant with in a determined dispatch period.

A simulation model of the hybrid MG, including real wind speed and solar irradiance data, was build and tested, showing the effectiveness of the proposed control strategy in different scenarios. Consequently, the proposed approach is a powerful tool to seamlessly integrate MGs in the ADN. In general, the proposed approach can integrate power ramp-rate limitation and power smoothing functionalities with the same battery capacity or even smaller. However, to implement additional peak-shaving operation, a larger battery capacity is needed.

A possible practical implementation should include local controllers for the different PV, WT, ESU power converters that may be implemented within a digital signal processor (DSP) platform, and a central controller that can be integrated into supervisory control and data acquisition (SCADA) system. The communication standard for data interchange is recommended to be based on the IEC 61850 (Ruiz-Alvarez 2012). Finally, the physical communication layer can be based on fiber optics, which may allow adding protection coordination schemes due to the fast transmission requirements.

References

Aalborg University, Photovoltaic Systems Research Programme: http://www.et.aau.dk/research-programmes/photovoltaic-systems/ Last access: March 2017.

Aalborg University, Microgrids Research Programme: www.microgrids.et.aau.dk Last access: March 2017.

Alam MJE, Muttaqi KM, and Sutanto D. A novel approach for ramp-rate control of solar PV using energy storage to mitigate output fluctuations caused by cloud passing. IEEE Transactions on Energy Conversion 2014, 29.2: 507-518.

Cai G, Kong L, Pan C, et al. System Modeling of Wind-PV-ES Hybrid Power System and Its Control Strategy for Grid-Connected. Transactions of China Electrotechical Society, 2013, 28(9): 123-128.

Chen B Y, Lai Y S. New digital-controlled technique for battery charger with constant current and voltage control without current feedback. IEEE Transactions on Industrial Electronics, 2012, 59(3): 1545-1553.

Cormode D, et al. Comparing ramp rates from large and small PV systems, and selection of batteries for ramp rate control. Photovoltaic Specialists Conference (PVSC), 2013 IEEE 39th. IEEE, 2013.

Díaz-González F, et al. Energy management of flywheel-based energy storage device for wind power smoothing. Applied energy 110 (2013): 207-219.

Fang X, et al. Coordinated dispatch in multiple cooperative autonomous islanded microgrids. Applied Energy 2016, 162: 40-48.

Gevorgian V, Booth S. Review of PREPA technical requirements for interconnecting wind and solar generation. National Renewable Energy Laboratory, National Renewable Energy Laboratory, Golden, CO, Technical Report No. NREL/TP-5D00-57089 (2013).

Guerrero JM, Vasquez JC, Matas J, Vicuna LG and Castilla M. Hierarchical Control of Droop-Controlled AC and DC Microgrids—A General Approach Toward Standardization. IEEE Transactions on Industrial Electronics, vol. 58, no. 1, pp. 158-172, Jan. 2011.

Haddadian H, Noroozian R. Multi-microgrids approach for design and operation of future distribution networks based on novel technical indices. Applied Energy 2017, 185: 650-663.

He Y, Hu J, Xu L. The operation control of grid-connected doubly fed induction generators. Beijing: China Electric Power Press, 2012.

Kim, Taesic, and Wei Qiao. A hybrid battery model capable of capturing dynamic circuit characteristics and nonlinear capacity effects. IEEE Transactions on Energy Conversion 26.4 (2011): 1172-1180.

Kim M, Kwasinski A. Decentralized Hierarchical Control of Active Power Distribution Nodes. IEEE Transactions on Energy Conversion, vol. 29, no. 4, pp. 934-943, Dec. 2014.

Lappalainen, Kari, and Seppo Valkealahti. Output power variation of different PV array configurations during irradiance transitions caused by moving clouds. Applied Energy 190 (2017): 902-910.

Lee, Hyewon, et al. Power-Smoothing Scheme of a DFIG Using the Adaptive Gain Depending on the Rotor Speed and Frequency Deviation. Energies 10.4 (2017): 555.

Li B, Shen H, Tang Y, and et al. Impacts of Energy Storage Capacity Configuration of HPWS to Active Power Characteristics and Its Relevant Indices. Power System Technology, 2011, 35(4): 196-204.

Liu N, et al. A hybrid forecasting model with parameter optimization for short-term load forecasting of micro-grids. Applied Energy 129 (2014): 336-345.

Liu W, Yang H, Zhu B. Survey on key technologies of microgrid. Power System Protection & Control, 2012(14):152-155.

Liu X, Jiang Q. An Optimal Coordination Control of Hybrid Wind/Photovoltaic/Energy Storage System. Automation of Electric Power System, 2012, 36(14): 95-100.

Luna, Adriana C, et al. Cooperative energy management for a cluster of households prosumers. IEEE Transactions on Consumer Electronics 62.3 (2016): 235-242.

Marzband M, et al. Experimental evaluation of a real time energy management system for stand-alone microgrids in day-ahead markets. Applied Energy 106 (2013): 365-376.

Ng K S, Huang Y F, Moo C S, et al. An enhanced coulomb counting method for estimating state-of-charge and state-of-health of lead-acid batteries. Telecommunications Energy Conference, 2009. INTELEC 2009. 31st International. IEEE, 2009: 1-5.

Niknam T, Azizipanah-Abarghooee R, Narimani MR. An efficient scenario based stochastic programming framework for multi-objective optimal microgrid operation. Applied Energy 2012;99:455–70.

Peng K, Liang D, and Gao L. Distributed EMPC of multiple microgrids for coordinated stochastic energy management. Applied Energy 2017, 185: 939-952.

Perdichizzi A, et al. Peak shaving strategy through a solar combined cooling and power system in remote hot climate areas. Applied Energy 143 (2015): 154-163.

Qi Y, Liu Y. Output Power Rolling Optimization and Real-Time Control in Wind-Photovoltaic-Storage Hybrid System. Transactions of China Electrotechnical Society, 2014, 29(8): 265-273.

Ren L, Bai Z, Yu C, and et al. Research on Active Power Control Strategy for Wind/Photovoltaic/Energy Storage Hybrid Power System and Its Engineering Application. Automation of Electric Power System, 2013, 28(9): 105-111.

Ruiz-Alvarez A, Colet-Subirachs A, Figuerola F A C, et al. Operation of a utility connected microgrid using an IEC 61850-based multi-level management system[J]. IEEE Transactions on Smart Grid, 2012, 3(2): 858-865.

Sang B, Wang D, Yang B, and et al. Optimal Allocation of Energy Storage System for Smoothing the Output Fluctuations of New Energy. Proceedings of the CSEE, 2014, 34 (22):3700-3706.

Shen J, Jiang C, Liu Y, & Qian, J. A Microgrid Energy Management System with Demand Response for Providing Grid Peak Shaving. Electric Power Components and Systems, 44(8), 843-852. (2016)

Song Z, Xia C, Shi T. Assessing transient response of DFIG based wind turbines during voltage dips regarding main flux saturation and rotor deep-bar effect. Applied Energy, 2010, 87(10): 3283-3293.

Vandoorn TL, Vasquez JC, De Kooning J, Guerrero JM, and Vandevelde L. Microgrids: Hierarchical Control and an Overview of the Control and Reserve Management Strategies. IEEE Industrial Electronics Magazine, vol. 7, no. 4, pp. 42-55, Dec. 2013.

Vasquez J C, Guerrero J M, Savaghebi M, et al. Modeling, analysis, and design of stationary-reference-frame droop-controlled parallel three-phase voltage source inverters[J]. IEEE Transactions on Industrial Electronics, 2013, 60(4): 1271-1280.

Wang C, Yu B, Xiao J, and et al. An Energy Storage System Capacity Optimization Method for Microgrid Tie-Line Power Flow Stabilization. Automation of Electric Power Systems, 2013, 37(3): 12-17

Wang D, et al. A Demand Response and Battery Storage Coordination Algorithm for Providing Microgrid Tie-Line Smoothing Services. IEEE Transactions on Sustainable Energy, vol. 5, no. 2, pp. 476-486, April 2014.

Wang R, Wang D, Jia H, and et al. A Coordination Control Strategy of Battery and Virtual Energy Storage to Smooth the Micro-grid Tie-line Power Fluctuations. Proceedings of the CSEE, 2015, 35(20):5124-5134.

Wang Y, Luo A, Jin G. Improved Robust Droop Multiple Loop Control for Parallel Inverters in Microgrid. Transactions of China Electrotechnical Society, 2015, 22:116-123.

Xiao J, Wang P, Setyawan L, Hierarchical Control of Hybrid Energy Storage System in DC Microgrids. IEEE Transactions on Industrial Electronics, vol. 62, no. 8, pp. 4915-4924, Aug. 2015.

Xiao Zhaoxia, Fan Shijun, Yang Qingxin. Research on Dynamically Improving the Power Factor of PCC Using Photovoltaic-Battery Generation System based on Hierarchical Control Strategy. Transactions of China Electrotechnical Society, 2015, 31(7): 107-117.

Zhao B, et al. An MAS based energy management system for a stand-alone microgrid at high altitude. Applied Energy 143 (2015): 251-261.

Zheng, Menglian, Christoph J. Meinrenken, and Klaus S. Lackner. Smart households: Dispatch strategies and economic analysis of distributed energy storage for residential peak shaving. Applied Energy 147 (2015): 246-257.

Zhou Kaile, Shanlin Yang, and Zhen Shao. Energy Internet: The business perspective. Applied Energy 178 (2016): 212-222.